ELSEVIER

Chemical Physics 233 (1998) 231–242

Chemical Physics

The intermolecular interaction mechanisms in liquid CS_2 at 295 and 165 K probed with two-dimensional Raman spectroscopy

A. Tokmakoff, M.J. Lang, X.J. Jordanides, G.R. Fleming *

Department of Chemistry and the James Franck Institute, University of Chicago, 5735 S. Ellis Ave., Chicago, IL 60637, USA

Received 20 October 1997

Abstract

Two-dimensional Raman spectroscopy is used to probe the intermolecular interaction dynamics of CS_2 at 295 and 165 K. The influence of nonlinear polarizability and liquid anharmonicity on the observable is discussed. It is found that the response at both temperatures is dominated by the nonlinear polarizability, which is most likely due to interaction-induced effects. A model using three Brownian oscillators to represent the collective motions on three time scales is unable to reproduce the 295 K data. At low temperature, the model presumably works better as a result of the time-scale separation between the inertial and diffusive dynamics.

1. Introduction

Building an understanding of physical processes and chemical reactions in condensed phases requires a microscopic description of dynamics between and within molecules. Since measurements of bulk (ensemble averaged) dynamics are not necessarily representative of all microscopic motions it is fundamentally difficult to draw conclusions about the molecular dynamics. More specifically, most measurements of bulk dynamics can be related to an ensemble-averaged two-point correlation function, or equivalently a frequency domain spectral density, which are necessarily insensitive to distributions or interactions within the ensemble [1–3]. Techniques in this category that probe the collective dynamics of condensed phases include all forms of light, X-ray, or neutron scattering, dielectric relaxation, far-infrared or terahertz absorption, and most spectroscopies on electronic chromophores [4]. To better characterize the molecular motions requires measurements that define the makeup of the ensemble and define interactions between particular dynamics or time-scales. This type of information requires measurements of a higher dimensionality, those techniques that probe three-point or higher order correlation functions for molecular motions [5].

Much recent interest has been focused on fifth order Raman spectroscopy for this reason [2,3,6–17]. It is a two-dimensional (2D) vibrational spectroscopy that allows the interactions between nuclear coordinates to be observed. Analogously to 2D NMR, the use of 2D Raman spectroscopy on well-defined high frequency vibrational motions allows the couplings between nuclear degrees of freedom to be quantified [12]. As an optical rephasing technique, it is also sensitive to heterogeneous dynamics [2,3]. In this paper the technique is used to study the mechanisms of intermolecular interactions in liquid CS_2.

* Corresponding author. Present address: Department of Chemistry, University of California, Berkeley, CA, 94720-1460, USA.

0301-0104/98/$19.00
PII: S0301-0104(98)00026-3

The 2D fifth order Raman experiment is shown schematically in Fig. 1. A series of five nonresonant femtosecond pulses are incident on a sample. These pulses are used to create multilevel vibrational coherences in all Raman active modes within the bandwidth of the excitation pulses, typically $< 500\ \mathrm{cm}^{-1}$. Two initial excitation pulses excite vibrational coherences $|a\rangle\langle b|$ at time t_0. After a delay time τ_2, a second Raman interaction allows the initial coherence to be transferred to new coherences involving a third state $|c\rangle$. The new coherence then evolves over a second period τ_4 until the fifth pulse probes it. Two possible interaction sequences corresponding to a rephasing and nonrephasing pathway are shown in Fig. 1b and c, respectively.

The existence of the fifth order signal is an indication that coherent superpositions between the $|a\rangle$, $|b\rangle$ and $|c\rangle$ states can be formed. In fact, a fifth order signal cannot be described by transitions on a single vibrational state, but requires the interaction of two states. This is reflected in the three-point polarizability correlation function that describes the fifth order Raman response [2]

$$\boldsymbol{R}^{(5)}(\tau_2,\tau_4) = -\frac{1}{\hbar^2}\left\langle\left[\left[\tilde{\alpha}(\tau_4+\tau_2),\tilde{\alpha}(\tau_2)\right],\tilde{\alpha}(0)\right]\right\rangle \qquad (1)$$

For any standard linear model based on harmonic oscillators this correlation function is zero. 2D Raman spectroscopy is a powerful technique primarily because of this two-state requirement. The existence of a fifth order signal implies a nonlinearity or coupling in the vibrational modes that are excited.

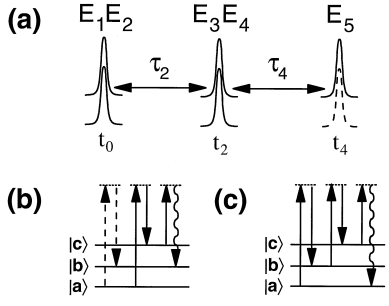

Fig. 1. (a) The time variables for the 2D fifth order Raman experiment. (b,c) Two representative ladder diagrams for processes contributing to the fifth order signal.

Two particular coupling mechanisms have been described as contributing to the fifth order signal: (1) A nonlinear dependence of the system polarizability on its nuclear coordinates, and (2) anharmonicity of the liquid potential [10–12,17]. The influence of these two interaction mechanisms on the signal characteristics of high frequency vibrational modes has been discussed previously [12–14,17]. Of particular interest now is the ability to distinguish these coupling mechanisms and their influence on intermolecular motions.

In this paper, we use 2D Raman experiments to study these interaction mechanisms in the intermolecular motions in CS_2 at room temperature and at 165 K. The emphasis is on understanding which intermolecular interaction mechanisms are present in liquid CS_2, and the effectiveness of the existing theoretical models for describing liquid dynamics. The nonlinear polarizability mechanism is found to be dominant in CS_2 at both temperatures. An asymmetry is present in the 2D responses that cannot be described by a small set of coupled Brownian oscillators, and indicates a need for an approach that reflects the continuous evolution of the liquid structure. At low temperature this model works better, presumably due to the time-scale separation between the inertial and diffusive dynamics. Previous fifth order Raman experiments on the intermolecular motions of CS_2 have interpreted the signal in terms of distributions of spatially varying dynamics in a manner that is similar to inhomogeneous line shape analysis [3,6–8]. Here, we show that these analyses are a special case of the coupling models described above and that the matrix of coupling elements is a measure of such effects.

2. Theoretical background

Of fundamental importance in obtaining molecular information from a Raman signal is relating the polarizability observable to nuclear coordinates. The generation of fifth order Raman signals is due to a nonlinearity in the vibrational modes excited in the experiment. In this paper we examine the two types of nonlinearity that have been proposed and explored theoretically for their relationship to the nuclear coordinates [10–12,18].

For discussing the origin of a Raman signal from a harmonic oscillator, it is common to postulate a weak linear dependence of the polarizability on a nuclear coordinate. In this case, the nested commutator (Eq. (1)) which describes the fifth order Raman signal vanishes. For the same harmonic system it is possible to postulate an origin to the fifth order signal by expanding the polarizability of the system in its coordinates

$$\tilde{\alpha} = \tilde{\alpha}(\boldsymbol{q}_0) + \sum_i \left(\frac{\partial\tilde{\alpha}}{\partial q_i}\right)_{q_0} q_i + \frac{1}{2}\sum_{ij}\left(\frac{\partial^2\tilde{\alpha}}{\partial q_i \partial q_j}\right)_{q_0} q_i q_j + \ldots \quad (2a)$$

$$= \alpha^{(0)} + \alpha_i^{(1)} q_i + \alpha_{ij}^{(2)} q_i q_j + \ldots \quad (2b)$$

Here, $\alpha^{(2)}$ is the first nonlinear polarizability expansion matrix. This expansion is inherently time-independent and therefore $\alpha^{(2)}$ is diagonally symmetric. Within the assumption that the expansion coefficients $\alpha_i^{(1)} \gg \alpha_{ij}^{(2)}$, one can show that the leading contributions to the signal arise from correlation functions which involve one two-quantum interaction. An example is $-\alpha_i^{(1)}\alpha_j^{(1)}\alpha_{ij}^{(2)} < [[q_i(\tau_2+\tau_4)q_j(\tau_2+\tau_4), q_i(\tau_2)], q_j(0)] > /\hbar^2$, in which the two initial interactions are one quantum transitions, while the probing step involves two. Such a process is pictured in Fig. 1c.

The nonlinearity in the vibration can also be introduced by introducing anharmonicity into the ground state Hamiltonian. If the potential is expanded about its minimum q_0, it can be shown that the dominant fifth order signal contributions arise from correlation functions that are proportional to the expansion coefficients of the cubic anharmonicity

$$V^{(3)} = \frac{1}{6}\sum_{ijk}\left(\frac{\partial^3 V}{\partial q_i \partial q_j \partial q_k}\right)_{q_0} q_i q_j q_k \quad (3a)$$

$$= g_{ijk}^{(3)} q_i q_j q_k \quad (3b)$$

Here, $g^{(3)}$ is the cubic anharmonicity tensor which is also symmetric to interchange of indices. The correlation functions in this case are of the form $g_{ijk}^{(3)}\alpha_i^{(1)}\alpha_j^{(1)}\alpha_k^{(1)} < [[q_i(\tau_2+\tau_4), q_j(\tau_2)], q_k(0)] >$, in which the coordinates q_i are now not in a harmonic basis but represent the anharmonically mixed states.

Under the circumstances described above, the dominant term in the third order response is given by a sum over the individual responses of the ensemble

$$R^{(3)}(\tau) = 2\sum_i \alpha_i^{(1)}\alpha_i^{(1)} C_i(\tau) \quad (4)$$

where C_i is the correlation function for a given vibrational mode. The same expression is obtained for a linear harmonic system. The nonlinearities described above contribute additional terms proportional to $\alpha_{ij}^{(2)}\alpha_{ij}^{(2)}$ and $g_{ijk}^{(3)}\alpha_j^{(1)}\alpha_{ij}^{(2)}$, which are assumed to be negligible.

Keeping only the leading terms, it can be shown that if both nonlinearities described are present, the fifth order response can be written as a sum of contributions due to the nonlinear polarizability and anharmonic potential of the system

$$R^{(5)}(\tau_2,\tau_4) = R_{\mathrm{NP}}^{(5)}(\tau_2,\tau_4) + R_{\mathrm{AN}}^{(5)}(\tau_2,\tau_4) \quad (5)$$

Each signal contribution is given by a sum over correlation functions

$$R_{\mathrm{NP}}^{(5)}(\tau_2,\tau_4) = \sum_{ij} R_{\mathrm{NP},ij}^{(5)}(\tau_2,\tau_4) \quad (6)$$

$$R_{\mathrm{AN}}^{(5)}(\tau_2,\tau_4) = \sum_{ijk} R_{\mathrm{AN},ijk}^{(5)}(\tau_2,\tau_4) \quad (7)$$

The individual 2D signal contributions are given by [18]

$$R_{\mathrm{NP},ij}^{(5)}(\tau_2,\tau_{(4)}) = 8\,\alpha_{ij}^{(2)}\alpha_i^{(1)}\alpha_j^{(1)} C_i(\tau_4) \times \big(C_j(\tau_2) + C_j(\tau_2+\tau_4)\big) \quad (8)$$

$$R_{\mathrm{AN},ijk}^{(5)}(\tau_2,\tau_4) = 48\, g_{ijk}^{(3)}\alpha_i^{(1)}\alpha_j^{(1)}\alpha_k^{(1)} \int_0^{\tau_4} \mathrm{d}\tau\, C_i(\tau_4-\tau) \times C_j(\tau) C_k(\tau_2+\tau) \quad (9)$$

From these expressions for the fifth order response it is clear that for a given set of basis modes, the 2D fifth order Raman response is described by a linear combination of their 2D responses weighted by the coupling elements $\alpha_{ij}^{(2)}$ or $g_{ijk}^{(3)}$.

Eq. (8) is a generalization of the previously derived fifth order response based on a nonlinear polarizability [2]. The interpretation of fifth order data within the traditional line shape classifications of 'homogeneous' and 'inhomogeneous' are limiting cases of these expressions. The inhomogeneous case is described by decoupling all basis modes that

describe the 1D response ($\alpha_{ij}^{(2)} = \delta_{ij}\alpha_i^{(1)}\alpha_j^{(1)}$), whereas the traditional homogeneous case is represented by fully coupling all modes ($\alpha_{ij}^{(2)} = \alpha_i^{(1)}\alpha_j^{(1)}$). The same limits hold for the anharmonic coupling case where the homogeneous and inhomogeneous limits are given by $g_{ijk}^{(3)} \propto \alpha_i^{(1)}\alpha_j^{(1)}\alpha_k^{(1)}$ and $g_{ijk}^{(3)} \propto \delta_{ij}\delta_{jk}\alpha_i^{(1)}\alpha_j^{(1)}\alpha_k^{(1)}$.

For interpreting the data below, we use the Brownian oscillator model, which allows qualitative description of collective intermolecular motions coupled to a harmonic bath, varying from overdamped to underdamped [5]:

$$C_i(\tau) = \eta_i \sin(\Omega_j \tau)\exp(-\Lambda_i \tau) \tag{10}$$

Here, $\eta_i = -\hbar/2m_i\Omega_i$, $\Omega_i = \sqrt{\omega_i^2 - \Lambda_i^2}$ is the reduced frequency, and $\Lambda_i = \gamma_i/2$ is the damping constant. Within this model, the temporal behavior of the nonlinear polarizability contribution is apparent from Eq. (8). The anharmonic contribution can be evaluated as

$$\begin{aligned} R_{\mathrm{AN},ijk}^{(5)}(\tau_2,\tau_4) &= 12\, g_{ijk}^{(3)}\alpha_i^{(1)}\alpha_j^{(1)}\alpha_k^{(1)}\eta_i\eta_j\eta_k \\ &\times \sum_{ab=\pm 1} \frac{\exp(-\Lambda_k\tau_2)}{\Gamma_{ijk}^2 + \xi_{ijk,ab}^2} \\ &\times \Big[ab\exp\big(-(\Lambda_k + \Lambda_j)\tau_4\big) \\ &\times \Big(\xi_{ijk,ab}\cos\big(\Omega_k(\tau_2+\tau_4) + b\Omega_j\tau_4\big) \\ &+ \Gamma_{ijk}\sin\big(\Omega_k(\tau_2+\tau_4) + b\Omega_j\tau_4\big)\Big) \\ &- b\exp(-\Lambda_i\tau_4)\Big(\xi_{ijk,ab}\cos(a\Omega_k\tau_2 + \Omega_i\tau_4) \\ &+ \Gamma_{ijk}\sin(a\Omega_k\tau_2 + \Omega_i\tau_4)\Big)\Big] \end{aligned} \tag{11}$$

with $\xi_{ijk,ab} = (\Omega_i - ab\Omega_j - a\Omega_k)$ and $\Gamma_{ijk} = (\Lambda_i - \Lambda_j - \Lambda_k)$.

In the limit of a single mode ($i = j = k$), Eq. (11) is equivalent to that derived previously [11,13]. The lack of temperature dependence to the anharmonic response arises from the assumption that the anharmonicity is a weak perturbation to the harmonic system.

Unlike 2D NMR, the Hamiltonian for describing vibrational systems in a 2D vibrational spectroscopy are significantly more complicated. The two vibrational mode interaction mechanisms described above are the only contributions that have been discussed thus far, but other coupling mechanisms should be investigated. While it can be argued that these effects may be small, it would still be important to investigate the role of Coriolis or centrifugal couplings on the 2D Raman experiment.

3. Experimental

One- and two-dimensional Raman experiments were performed with a regeneratively amplified Ti:sapphire laser producing Gaussian pulses of 47 fs duration at 3.8 kHz [19]. This pulse duration gives a broad enough bandwidth to excite all intermolecular motions in CS_2, but not intramolecular vibrations. All measurements were made with parallel polarizations. One-dimensional Raman responses of the intermolecular motions of CS_2 were taken using a nonresonant pump-probe experiment. A 0.5 μJ pump and probe beam were focused with a 30 cm singlet to 270 μm in a 1 mm fused silica cuvette of multiply filtered CS_2. The pump beam was chopped at 1.9 kHz and the modulation of the probe beam amplitude at that frequency was detected with a lock-in amplifier.

Fifth order Raman signals were detected using an intrinsic heterodyne detection geometry that has been described in detail previously [20]. Rather than measuring the modulus squared response $|R^{(5)}(\tau_2,\tau_4)|^2$, this sensitive technique measures the cross term $R^{(3)}(\tau_4)R^{(5)}(\tau_2,\tau_4)$. The same focusing optic was used and the combined beam energy for these measurements was 2 μJ. The data was collected by sweeping τ_2 from 200 to >1500 fs for fixed values of τ_4, and then stepping τ_4 from -200 to >1200 fs for a total data collection time of ca. 14 h.

Data for CS_2 just above its freezing point was taken with a closed cycled helium refrigerator. The CS_2 sample was held in brass cell of 0.4 mm path length with fused silica windows. The temperature of the cell was regulated at 165 ± 1 K over the data collection time. The additional material of the sample cell and cold-jacket windows were precompensated for to maintain the time resolution.

4. Results and discussion

Fig. 2 shows the polarized 1D Raman responses $R^{(3)}(\tau)$ for CS_2 at 295 and 165 K. At both tempera-

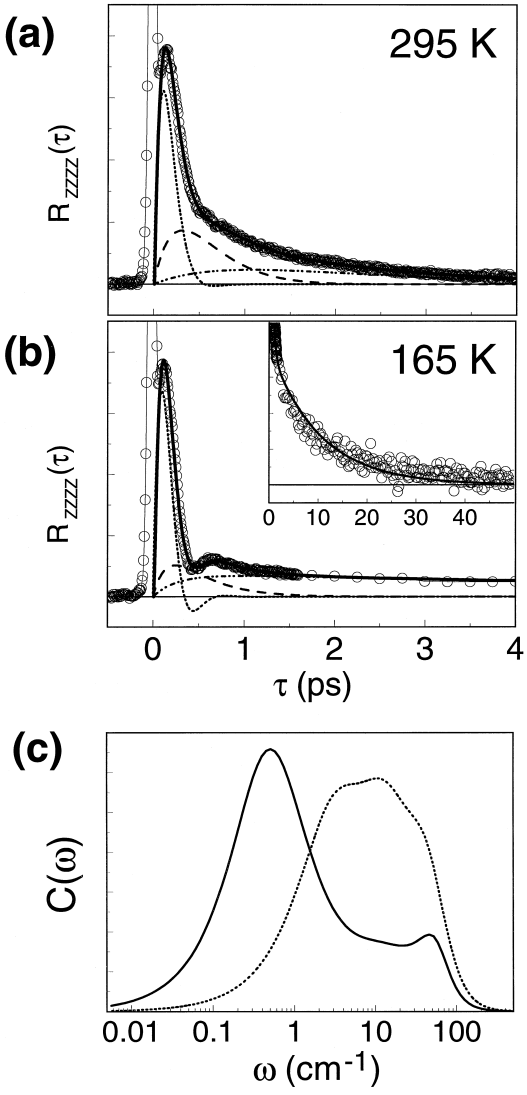

Fig. 2. 1D third order Raman response $R^{(3)}_{ZZZZ}$ of CS_2 at (a) 295 and (b) 165 K. Also shown are the three Brownian oscillator modes to which the responses are fit. The inset to (b) shows the long time decay at 165 K. (c) The spectral density representation obtained from the sine transform of the time domain fits above: (dash) 295 and (solid) 165 K.

tures the data show a pulse limited electronic contribution at $\tau = 0$ followed by the inertial response of the liquid to the impulsive excitation. The inertial response damps rapidly to diffusive behavior. In the low temperature case, the response is somewhat underdamped, with a clear oscillation. In the long time limit (> 4 ps) the decay is exponential with time constants of 1.65 and 10.6 ps at 295 and 165 K, respectively. These results are in agreement with previous temperature dependent experiments of the Raman response of CS_2 [21–24].

Table 1
Parameters for the fit of three Brownian oscillators (Eq. 10) to the 1D Raman response from CS_2 shown in Figure 2

T (K)	Mode	α_i	ω_i (cm^{-1})	γ_i(cm^{-1})
295	1	28.5	53.9	89.7
	2	8.73	16.9	31.6
	3	2.53	4.8	10.4
165	1	28.1	60.0	72.6
	2	8.21	20.9	45.0
	3	4.04	3.35	23.0

The 1D response from CS_2 at room temperature has been widely studied [1], with a common observation. There are effectively three time scales present in the response. The inertial component damps in < 500 fs and the diffusive component does not reach exponential behavior until > 2 ps. The remaining dynamics belong to an intermediate time scale. On this basis it is common to fit the response to the sum of three collective oscillators with these characteristic time scales. The fit of both 1D decays to three Brownian oscillators is also shown in Fig. 2, and the fit parameters are summarized in Table 1. For the following discussion the inertial, intermediate, and diffusive components are referred to as modes 1, 2 and 3, respectively. The spectral density representation of these data sets is shown in Fig. 2c as the sine transform of the fits to the 1D impulse response. This shows the separation of the inertial and diffusive components on cooling the sample.

The 2D $R^{(3)}(\tau_4)R^{(5)}(\tau_2,\tau_4)$ responses from CS_2 at both temperatures are shown in Fig. 3. A ridge that extends along τ_2, centered at $\tau_4 \approx 150$ fs dominates the response at both temperatures. The maximum value for τ_4 corresponds to the peak of the inertial component in the 1D response. At both temperatures the decays along τ_4 are much faster than along τ_2. The slice out of the response along τ_2 for $\tau_4 \approx 150$ fs is qualitatively the same as the 1D response.

[1] The many studies of the room temperature response from CS_2 have been reviewed in Ref [25].

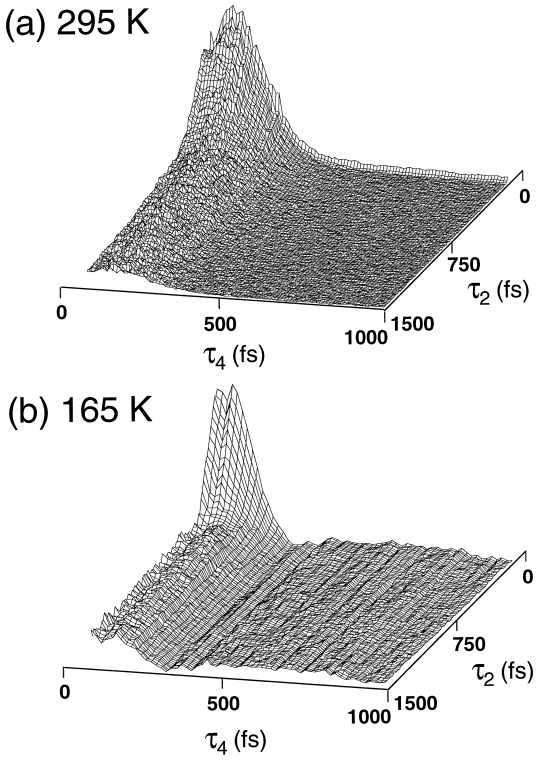

Fig. 3. 2D heterodyne-detected Raman response $R^{(3)}_{ZZZZ}(\tau_4)R^{(5)}_{ZZZZZZ}(\tau_2,\tau_4)$ of CS_2 at (a) 295 and (b) 165 K. The strong hyperpolarizability signals that are present for τ_2 and $\tau_4 < 60$ fs have been truncated in this presentation, since they do not contain 2D information.

The characteristic differences between the two data sets lie in the long time behavior. Whereas the 295 K signal has vanished by $\tau_4 = 500$ fs, in the 165 K data a dip, slight rise, and ps decay is observed for $\tau_4 > 300$ fs at all values of τ_2 measured. The low amplitude ridge is peaked at $\tau_4 \approx 600$ fs and is an indication that nonzero fifth order signals are observed to large (ps) delays of τ_2 and τ_4. The observation of the ridges and trenches along τ_2 is most likely a result of the beat in the third order response manifesting itself in the $R^{(3)}(\tau_4)R^{(5)}(\tau_2,\tau_4)$ cross term data, although the minimum in the 1D signal and the trench position in the 2D data do not exactly coincide.

To describe the interaction dynamics in the CS_2 intermolecular motions, we use the three-oscillator parameterization of the CS_2 dynamics to which the 1D data was fit. This parameterization does not necessarily represent a division into particular nuclear motions, but rather serves to group the collective motions of the liquid into particular time scales. The interpretation of couplings in the 2D data is therefore interpreted as the interactions between intermolecular motions on particular time scales. The choice of three modes is entirely arbitrary and any number of modes could be used. Three is the minimum number that we can use to adequately describe the 1D data, and allows certain general conclusions about the 2D data to be drawn.

To investigate the influence of molecular interactions due to the nonlinear polarizability on the 2D Raman signal, we plot the 2D correlation functions $R^{(5)}_{NP,ij}(\tau_2,\tau_4)$ for the individual nonlinear polarizability coupling matrix elements $\alpha^{(2)}_{ij}$ where the subscripts label the oscillators. Fig. 4 shows the 2D response $R^{(5)}_{NP,ij}(\tau_2,\tau_4)$ from each of the nine elements of $\alpha^{(2)}$ for the three oscillators fit to the 1D CS_2 data at 295 K. The fifth order signal for the case of coupling due purely to the nonlinear polarizability is described by a linear combination of these responses weighted by $\alpha^{(2)}_{ij}$. The individual 2D responses are elongated along τ_2 for $i<j$, along τ_4 for $i>j$, and are almost symmetric for $i=j$. The temporal behavior can be interpreted by the correlation functions in Eq. (8). The j index represents the coherent state in which the system evolves during the first time interval, and the i index indicates the superposition state into which the initial coherence is promoted by the second interaction. The rise and decay characteristics along the τ_2 and τ_4 axes are mostly dictated by the dynamics of the j and i modes, respectively. Although a direct comparison between the calculated $R^{(5)}_{NP,ij}(\tau_2,\tau_4)$ and the heterodyne data is not possible, it is still evident that elements with $j=0$ resemble the ridge along τ_2 in the 2D Raman data. Although individual elements may resemble the response, it is important to note that experimentally there is no selectivity to a particular correlation function.

As with the nonlinear polarizability, mode couplings due to the vibrational anharmonicity are also described by a linear combination of responses $R^{(5)}_{AN,ijk}(\tau_2,\tau_4)$ weighted by the individual tensor elements of the cubic anharmonicity $g^{(3)}_{ijk}$. Using the expression for $R^{(5)}_{AN,ijk}(\tau_2,\tau_4)$ in Eq. (11), the contributions to the 2D response from each of the given

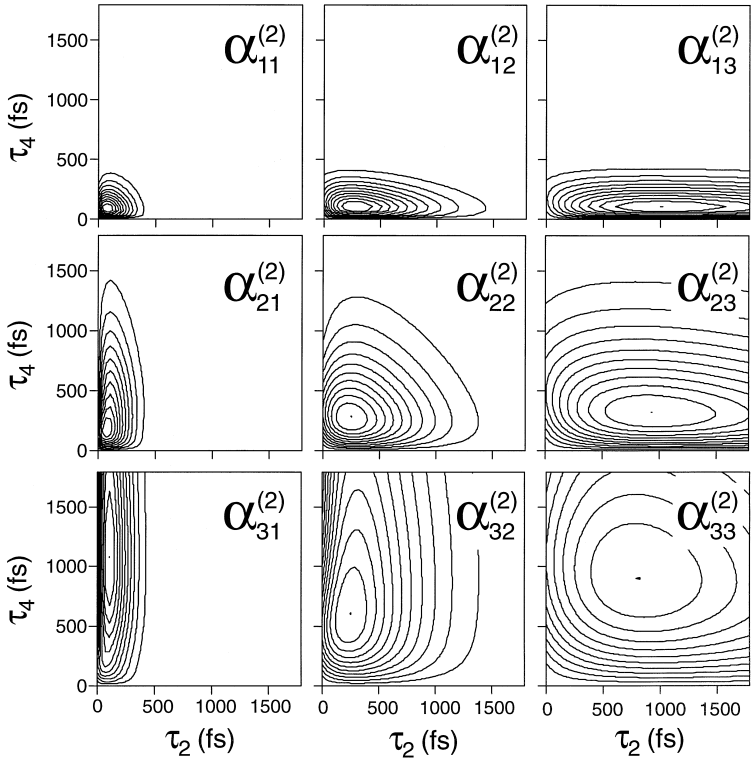

Fig. 4. Calculated 2D response $R^{(5)}_{\mathrm{NP},ij}(\tau_2,\tau_4)$ for the nine elements of the nonlinear polarizability coupling matrix $\alpha^{(2)}$ in the three mode system derived from the fit to the 295 K CS_2 data in Fig. 2a. The contours are drawn in 10% of maximum intervals.

anharmonic tensor elements involving the interaction between the inertial and intermediate time scales are plotted in Fig. 5. The 2D response from a single anharmonic mode $g^{(3)}_{iii}$ is qualitatively the same as those that were calculated previously [11,13].

The contours of the anharmonic responses have markedly different characteristics from those in Fig. 4. Unless $k > j$, the maximum signal is observed for $\tau_2 = 0$ rather than for positive values of τ_2 and τ_4. Again the temporal behavior in the correlation function is dictated by the ordering of the indices. The k index represents the mode that is initially excited, and dictates the rate of decay with τ_2. The i index is for the final state occupied, and dictates the decay along τ_4. Both j and k indices dictate the rise time along τ_4.

The significant difference between the anharmonic and nonlinear polarizability responses are the characteristic rise times for slices along τ_4. Although the 2D contribution from the anharmonic tensor elements $g^{(3)}_{11k}$ have the same elongation along the τ_2 axis observed in the 2D Raman, the ridges in these responses lie at longer delays ($\tau_4 \approx 250$ fs than in the case of the nonlinear polarizability ($\tau_4 \approx 150$ fs). Fig. 6 shows a comparison of the rise times of the fastest nonlinear polarizability and anharmonicity components $\alpha^{(2)}_{12}$ and $g^{(3)}_{112}$ with the 2D data along τ_4. The nonlinear polarizability contribution rises rapidly and represents the short time behavior along τ_4 well, but the anharmonic contribution rises too slowly. Clearly, the anharmonic contribution cannot itself reproduce the data, and must be at most a small contribution to the fifth-order signal from CS_2. The same conclusions can be drawn from the low temperature CS_2 data. The dominance of the nonlinear polarizability contribution allows no observation to be made on the temperature dependence of the intermolecular anharmonicity. On the basis of a single mode fit to room temperature homodyne data [3], Okumura and Tanimura have found anharmonicity is present in the 2D Raman response from CS_2 [11].

It is not surprising that interactions due to the

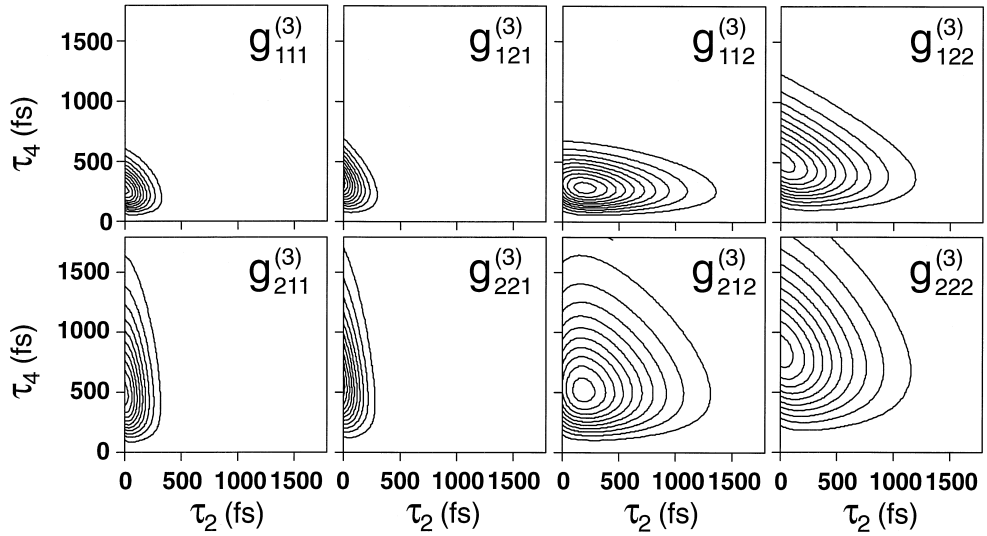

Fig. 5. Calculated 2D response $R^{(5)}(\tau_2,\tau_4)$ from the eight cubic anharmonicity tensor elements $g^{(3)}_{ijk}$ involving the interactions between the inertial (1) and intermediate (2) modes from the fit to the 295 K CS_2 data in Fig. 2a. The contours are drawn in 10% of maximum intervals. The top and bottom rows show the responses for $i=1$ and $i=2$. The two left columns show responses for $k=1$ while those on the right are for $k=2$.

nonlinear polarizability of CS_2 dominate the 2D Raman data. CS_2 has extremely high isotropic and anisotropic intermolecular polarizabilities. Previous molecular dynamics simulations of the CS_2 intermolecular dynamics have concluded that most significant signal contributions to the short time dynamics of 1D observables arise from interaction-induced effects [21,26–28]. Interaction-induced effects, in which the motions of one molecule distort the electronic states of a neighboring molecule, are perhaps the most significant intermolecular interactions that are described in terms of a nonlinear polarizability.

In the limit that the ensemble-averaged response

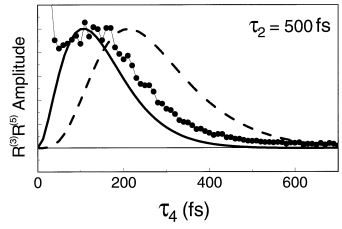

Fig. 6. Comparison the 2D heterodyne Raman data for $\tau_2 = 500$ fs (circles) with the response functions $R^{(3)}(\tau_4)R^{(5)}(\tau_2,\tau_4)$ for the nonlinear polarizability and anharmonicity components $\alpha^{(2)}_{12}$ (solid) and $g^{(3)}_{112}$ (dash).

describes the microscopic dynamics at all points in the liquid, and the strength of interaction between motions on different time scales is proportional to their respective amplitudes, the signal is described by the homogeneous limit. Fig. 7 shows a calculation of the expected heterodyne responses for both coupling mechanisms and both temperatures in this limit. As expected, the calculations based on the anharmonicity do not reproduce the placement of the characteristic ridge along τ_2 or the signal profile for small τ_2. The nonlinear polarizability calculations approximately reproduce the ridge along τ_2, however, the decay characteristics along τ_4 are not good. A distinct ridge, which is not present in the data, appears along the τ_4 axis at $\tau_2 \approx 150$ fs in the 295 K calculation. The appearance of this ridge, due to the high amplitude of the $\alpha^{(2)}_{i1}$ elements, has been discussed in previous modeling of the room temperature CS_2 data [3]. In the 165 K data, the amplitude of the calculated signal is too low for $\tau_2 > 300$ fs, and is essentially nonexistent for $\tau_4 > 350$ fs. These differences between these calculations and the 2D data are the basis for investigating deviations from homogeneous behavior.

Further insight into the interactions between motions on different time scales can be made with a fit

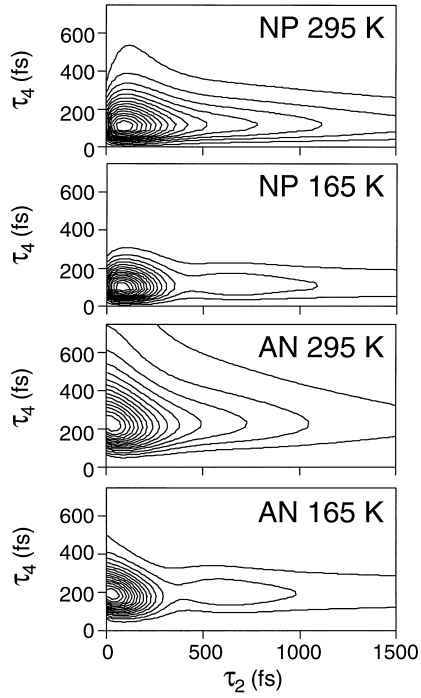

Fig. 7. Calculations of the heterodyne response $R^{(3)}(\tau_4)R^{(5)}(\tau_2,\tau_4)$ at 295 K and 165 K for the nonlinear polarizability (NP) and anharmonic (AN) models, using homogeneous coupling tensors, $\alpha^{(2)}_{ij} = \alpha^{(1)}_i\alpha^{(1)}_j$ or $g^{(3)}_{ijk} \propto \alpha^{(1)}_i\alpha^{(1)}_j\alpha^{(1)}_k$. Contours are drawn in 6.7% intervals.

to the 2D data. Since the data sets appear to be dominated by the effects of the nonlinear polarizability, both 2D data sets were fit to the a sum of contributions from the six independent elements of the $\alpha^{(2)}$ matrix, as described by Eqs. (6) and (8). The fits, pictured in Fig. 8, were made directly to the heterodyne data using a 2D least squares fitting algorithm. Table 2 shows the relative amplitudes of the $\alpha^{(2)}$ matrix elements at both temperatures. The fit to the 295 K data reproduces the features of the data along the τ_2 ridge but again contains the extra ridge in the τ_4 dimension. It should be noted that differences between the fit and data along τ_4 may seem small due to the biasing effect of the third order signal in the $R^{(3)}(\tau_4)R^{(5)}(\tau_2,\tau_4)$ heterodyne signal; however, the differences are in fact quite significant. This additional ridge highlights an inherent asymmetry in the data that cannot be accounted for with the necessary symmetry of the $\alpha^{(2)}$ matrix in the time-independent coupled mode model used here.

The features of the 165 K data can be better reproduced. The fit yields a signal that contains the overall characteristics of a trench and second ridge for long τ_4 delays, in addition to the ridge characteristics along τ_2. There are still problems with reproducing the amplitudes of the various features and the position of the trench, but a significant part of this lies in the small set of basis oscillators used. The primary factor in reproducing the long delay characteristics of the data is the dominant value of the $\alpha^{(2)}_{33}$ element in the $\alpha^{(2)}$ matrix. Unlike the 295 K data, there are only small difficulties in using a symmetric $\alpha^{(2)}$ matrix to fit the 165 K data. This is a significant

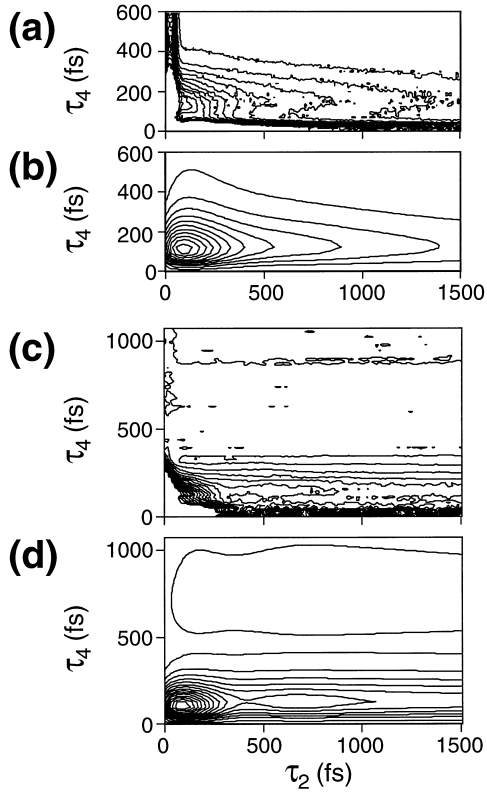

Fig. 8. Comparison of the 2D Raman data shown in Fig. 3 and fits using the nonlinear polarizability response model: (a,b) 295 and (c,d) 165 K. The contours in (a,b) are drawn in 9% intervals of the amplitude at $\tau_2 = \tau_4 = 100$ fs, while those in (c,d) are drawn in 6.7% intervals. The strong signal contributions in the data along the time axis for t_2 or $t_4 = 0$ are due to 1D hyperpolarizability contributions to the signal.

Table 2
The values of the matrix elements $\alpha_{ij}^{(2)}$ relative to the maximum value based on a fit to the heterodyned 2D fifth order Raman data. These are the average values based on a number of 2D least squares fits. The error bars are approximately 10% for values > 0.5, 20% for values > 0.1 and larger for lower values

	295 K			165 K		
i, j	1	2	3	1	2	3
1	1	0.28	0.12	0.81	0.282	0.232
2	0.28	0.19	0.088	0.282	0.044	0.036
3	0.12	0.088	0.002	0.232	0.036	1

difference, implying that the inherent temporal asymmetry observed in the room temperature data is much smaller in the low temperature data.

From our discussion of the limiting homogeneous and inhomogeneous forms of the $\alpha^{(2)}$ matrix, it should be evident that the form of this matrix gives information on the sample heterogeneity. The classical inhomogeneous line shape arises when fast dynamics of an ensemble are decoupled from each other. The lack of interaction between motions in the formalism of the nonlinear polarizability implies a diagonal $\alpha^{(2)}$ matrix. High amplitude in the diagonal $\alpha^{(2)}$ elements is in many ways equivalent to the observation of a temporal echo in the data.

To be more general, in a liquid it is of interest to see to what extent modes interact with themselves as opposed to others. This can be measured by comparing the amplitude of diagonal elements of $\alpha^{(2)}$ to the off-diagonal ones. At room temperature the value of the diagonal elements seem to track the amplitude of neighboring off-diagonal elements. This is an indication that there is no preferential self-correlation for motions, and that the environment has little heterogeneity. However at 165 K, the dominant element in the low temperature data is $\alpha_{33}^{(2)}$, the longest time diagonal component. The high amplitude of this component suggests that on a 1–2 ps time scale there is still heterogeneity in the diffusive response of the liquid. To be more quantitative it will be necessary to investigate the low temperature system at longer times, and with a homodyne detection geometry to remove the biasing effect of the third order signal.

The requirement of a symmetric nonlinear polarizability coupling tensor arises from a time-independent expansion of the polarizability in terms of collective oscillators used to represent the nuclear coordinates of the liquid. Such an expansion, while common for describing intramolecular vibrational spectra, is not necessarily appropriate for liquids where the collective modes may time-dependent. This is clear from normal mode models which work well for the short time dynamics (typically < 300 fs), but fail to capture the longer time scale motions which include crossing of potential barriers and the large scale restructuring of the molecules. It is less obvious that the collective Brownian oscillators would fail to describe the 2D data.

A clear result from Fig. 8 is that the coupled collective oscillator model can fit the data better at lower temperatures. In other words, a symmetric $\alpha^{(2)}$ appears to work better. We believe the arises from a larger separation of inertial and diffusive motions at low temperature so that time-independent oscillators would be approximately defined. In room temperature liquids, the time scales of the various motions vary continuously from inertial to diffusive, and even the collective Brownian oscillators evolve in time. As seen in Fig. 2c, as the sample is cooled the strong inertial response becomes clearly separated from the much slower diffusive motions, and it seems reasonable to expect that the liquid dynamics encompassed by these motions become effectively decoupled through the time scale separation. In this limit, describing the collective coordinates associated with these motions as essentially time-independent is adequate, and grouping the time scales of the response into particular oscillators is more physically realistic.

At high temperatures it is apparent that the use of the time-independent expansion is inadequate for room temperature liquids. The 2D Raman data exhibits a clear temporal asymmetry that cannot be accounted for within this model. The room temperature data can only be fit in the context of the present model if $\alpha_{ij}^{(2)} \neq \alpha_{ji}^{(2)}$. Such breaking of the symmetry of the current Hamiltonian could only occur if the collective oscillators evolve in time.

A parallel picture to the one given above has been suggested for polymer glasses and polar liquids as a result of resonant photon echo experiments [29–31]. In the dye/polymer glass systems the linearly coupled harmonic bath combined with static inhomogeneous broadening accurately describes the linear and nonlinear spectroscopy from 30 to 300 K [29,31]. In

other words, a temperature independent spectral density and a temperature independent inhomogeneous width quantitatively describe the data. In the liquid ethylene glycol, the inhomogeneous broadening has now become the diffusive component of the solvation dynamics and a temperature-independent spectral density no longer suffices, especially at low frequencies, suggesting a separation into librational and diffusive time scales is no longer realistic [30].

Saito and Ohmine have used normal mode calculations to investigate the origin of the fifth order Raman signal from CS_2 at 300 K [16]. In their results, mode coupling plays an important role in describing the observed response. With both instantaneous and quenched normal modes, significant inhomogeneity is observed as the formation of an echo along $\tau_2 = \tau_4$ after averaging over > 40 configurations. Although this feature is not observed in our data, the amplitude of the echo in mode-coupled simulations was significantly decreased from mode-decoupled simulations. In a spectral analysis, they also found that the higher frequency components particularly near 30 and 80–100 cm^{-1} were strongly self-coupled. Although our results of fitting $\alpha^{(2)}$ predict a strong degree of self-coupling for frequency components > 30 cm^{-1}, we presume that improved models will show asymmetric couplings involving lower frequency motions. Lower frequency couplings are not seen in the calculation of Saito and Ohmine because harmonic normal mode analyses do not incorporate the diffusive dynamics.

5. Concluding remarks

The 2D fifth order intermolecular Raman response from CS_2 is dominated at both temperatures by nonlinear polarizability effects. These signal contributions are likely due to interaction-induced effects, since these effects are significant in the 1D dynamics of CS_2. While the role of anharmonicity in this response is not ruled out, it can be at most a small contribution to the signal in the time range studied. Interpreting the results in terms of interactions between motions on different time-scales shows that at room temperature, motions of all time-scales appear to couple effectively to each other. We believe that our inability to reproduce the 295 K data results from the assumption of time-independent collective coordinates. At low temperature, the motions seem separable and a model based on three coupled Brownian oscillators works reasonably well.

The use of the analysis presented here highlights the importance of 2D spectroscopy in understanding the intermolecular interactions of liquids. Our previous experiments on the interaction between intramolecular modes in CCl_4 and $CHCl_3$ showed how couplings between well-defined vibrations could be observed [12]. The present experiments show how the same information content is present in studies of the intermolecular dynamics. More sophisticated models than the one used here should provide considerable insight into the molecular motions of liquids.

Acknowledgements

The authors thank Prof. Shaul Mukamel and Dr. Vladimir Chernyak for valuable discussions on the nature of couplings in the fifth order Raman experiment, and for pointing out an error in an earlier version of this manuscript. We also acknowledge important discussions and preprints received from Prof. M. Cho, Dr. K. Okumura, and Dr. S. Saito. This research was supported by a grant from the National Science Foundation. A.T. thanks the National Science Foundation for a postdoctoral research fellowship. M.J.L. is a GAAN fellow.

References

[1] G.R. Fleming, M. Cho, Annu. Rev. Phys. Chem. 47 (1996) 109–134.
[2] Y. Tanimura, S. Mukamel, J. Chem. Phys. 99 (1993) 9496.
[3] A. Tokmakoff, G.R. Fleming, J. Chem. Phys. 106 (1997) 2569.
[4] B.J. Berne, R. Pecora, Dynamic Light Scattering, Krieger, Malabar, FL, 1990.
[5] S. Mukamel, Principles of Nonlinear Optical Spectroscopy, Oxford University Press, New York, 1995.
[6] V. Khidekel, S. Mukamel, Chem. Phys. Lett. 240 (1995) 304; V. Khidekel, V. Chernyak, S. Mukamel, J. Chem. Phys. 105 (1996) 8543.
[7] K. Tominaga, K. Yoshihara, Phys. Rev. Lett. 171 (1995) 179; J. Chem. Phys. 104 (1996) 4419; J. Chem. Phys. 104 (1996) 1159; K. Tominaga, G.P. Keogh, Y. Naitoh, K.

Yoshihara, J. Raman Spectrosc. 26 (1995) 495; K. Tominaga, Adv. Multi-Photon Process. Spectrosc. 11 (1997) 1.
[8] T. Steffen, K. Duppen, Phys. Rev. Lett. 76 (1996) 1224; T. Steffen, J.T. Fourkas, K. Duppen, J. Chem. Phys. 105 (1996) 7364; T. Steffen, K. Duppen, J. Chem. Phys. 106 (1997) 3854.
[9] A. Tokmakoff, J. Chem. Phys. 105 (1996) 13.
[10] K. Okumura, Y. Tanimura, J. Chem. Phys. 106 (1997) 1687.
[11] K. Okumura, Y. Tanimura, J. Chem. Phys. 107 (1997) 2267.
[12] A. Tokmakoff, M.J. Lang, D.S. Larsen, G.R. Fleming, V. Chernyak, S. Mukamel, Phys. Rev. Lett. 79 (1997) 2702.
[13] K. Okumura, Y. Tanimura, Chem. Phys. Lett. 277 (1997) 159.
[14] K. Okumura, Y. Tanimura, Chem. Phys. Lett. 278 (1997) 175.
[15] R.L. Murry, J.T. Fourkas, J. Chem. Phys. 107 (1997) 9726.
[16] S. Saito, I. Ohmine, J. Chem. Phys. 107 (1998) 240.
[17] M. Cho, K. Okumura, Y. Tanimura, J. Chem. Phys. 108 (1998) 1326.
[18] A. Tokmakoff, M.J. Lang, D.S. Larsen, G.R. Fleming, V. Chernyak, S. Mukamel, J. Chem. Phys., in preparation.
[19] T. Joo, Y. Jia, G.R. Fleming, Opt. Lett. 20 (1995) 389.
[20] A. Tokmakoff, M.J. Lang, D.S. Larsen, G.R. Fleming, Chem. Phys. Lett. 272 (1997) 48.
[21] T.I. Cox, M.R. Battaglia, P.A. Madden, Mol. Phys. 38 (1979) 1539.
[22] S. Ruhman, K.A. Nelson, J. Chem. Phys. 94 (1991) 859.
[23] R.A. Farrer, B.J. Loughnane, J.T. Fourkas, J. Chem. Phys. 106 (1997) 6901.
[24] R.A. Farrer, B.J. Loughnane, J.T. Fourkas, J. Phys. Chem. A 101 (1997) 4005.
[25] D. McMorrow, N. Thantu, J.S. Melinger, S.K. Kim, W.T. Lotshaw, J. Phys. Chem. 100 (1996) 10389.
[26] P.A. Madden, D.J. Tildesley, Mol. Phys. 55 (1985) 969.
[27] L.C. Geiger, B.M. Ladanyi, Chem. Phys. Lett. 159 (1989) 413.
[28] L.C. Geiger, B.M. Ladanyi, J. Chem. Phys. 87 (1987) 191.
[29] Y. Nagasawa, S.A. Passino, T. Joo, G.R. Fleming, J. Chem. Phys. 106 (1997) 4640.
[30] S.A. Passino, Y. Nagasawa, G.R. Fleming, J. Chem. Phys. 107 (1997) 6094.
[31] Y. Nagasawa, J.-Y. Yu, G.R. Fleming, J. Chem. Phys., submitted for publication.